
Article:
Hao, J., Zeltz, C., Pintilie, M. et al. (15 more authors) (2019) Characterization of Distinct Populations of Carcinoma-Associated Fibroblasts from Non-Small Cell Lung Carcinoma Reveals a Role for ST8SIA2 in Cancer Cell Invasion. Neoplasia, 21 (5). pp. 482-493. ISSN 1522-8002

https://doi.org/10.1016/j.neo.2019.03.009

NEOPLASIA
www.neoplasia.com

Volume 21 Number 5 May 2019 pp. 482–12493 **482**

Characterization of Distinct Populations of Carcinoma-Associated Fibroblasts from Non–Small Cell Lung Carcinoma Reveals a Role for ST8SIA2 in Cancer Cell Invasion[1,2]

Jing Hao[*,3], Cédric Zeltz[†,3], Melania Pintilie[†], Quan Li[†], Shingo Sakashita[†], Tao Wang[†], Michael Cabanero[†], Sebastiao N. Martins-Filho[†], Dennis Y. Wang[‡], Elena Pasko[†,§], Kalpana Venkat[†], Joella Joseph[†,¶], Vibha Raghavan[†], Chang-Qi Zhu[†], Yu-Hui Wang[†], Nadeem Moghal[†,¶], Ming-Sound Tsao[†,§,¶,#] and Roya Navab[†]

[*]Cancer Center, Qilu Hospital of Shandong University, Jinan, China; [†]Princess Margaret Cancer Center, University Health Network, Toronto, Ontario, Canada; [‡]Sheffield Institute of Translational Neuroscience, University of Sheffield, Sheffield, UK, S1O 2HQ; [§]Laboratory Medicine and Pathobiology, Toronto, Ontario, Canada; [¶]Departments of Medical Biophysics, Toronto, Ontario, Canada; [#]Ontario Institute of Cancer Research, Toronto, Ontario, Canada

Abstract

Carcinoma-associated fibroblasts (CAFs) are abundant stromal cells in tumor microenvironment that are critically involved in cancer progression. Contrasting reports have shown that CAFs can have either pro- or antitumorigenic roles, indicating that CAFs are functionally heterogeneous. Therefore, to precisely target the cancer-promoting CAF subsets, it is necessary to identify specific markers to define these subpopulations and understand their functions. We characterized two CAFs subsets from 28 non–small cell lung cancer (NSCLC) patient tumors that were scored and classified based on desmoplasia [mainly characterized by proliferating CAFs; high desmoplastic CAFs (HD-CAF; $n = 15$) and low desmoplastic CAFs (LD-CAF; $n = 13$)], which is an independent prognostic factor. Here, for the first time, we demonstrate that HD-CAFs and LD-CAFs show different tumor-promoting abilities. HD-CAFs showed higher rate of collagen matrix remodeling, invasion, and tumor growth compared to LD-CAFs. Transcriptomic analysis identified 13 genes that were differentially significant (fold ≥ 1.5; adjusted P value $< .1$) between HD-CAFs and LD-CAFs. The top upregulated differentially expressed gene, *ST8SIA2* (11.3 fold; adjusted P value $= .02$), enhanced NSCLC tumor cell invasion in 3D culture compared to control when it was overexpressed in CAFs, suggesting an important role of ST8SIA2 in cancer cell invasion. We confirmed the protumorigenic role of ST8SIA2, showing that ST8SIA2 was significantly associated with the risk of relapse in three independent NSCLC clinical datasets. In summary, our studies show that functional heterogeneity in CAF plays key role in promoting cancer cell invasion in NSCLC.

Neoplasia (2019) 21, 482–493

Address all correspondence to: Roya Navab, Princess Margaret Cancer Research Tower / University Health Network, 101 College St. 11th Floor / Rm 11-301AM, Toronto, ON, M5G 1L7. E-mail: Roya.Navab@uhnresearch.ca

[1] Conflicts of interest: The authors declare no potential conflicts of interest.

[2] Author contributions statement: R. N, C. Z., and M. S. T. designed research. R. N., C. Z., J. H., Y. W., E. P., K. V., and J. J. performed research. S. S., T. W., M. C., and S. M. F. assessed the histological features in tumors and provided the clinical data. D. W., Q. L., V. R., and C. Z. carried out the bioinformatics data analysis. M. P. carried out statistics analysis. R. N., C. Z., M. P., S. M. F., N. M., and M. S. T. wrote the paper.

[3] J. H. and C. Z. contributed equally to this work.

Received 23 October 2018; Revised 15 March 2019; Accepted 21 March 2019

1476-5586

Introduction

Tumor stroma is no longer seen solely as physical support for mutated epithelial cells but as an important modulator and even a driver of tumorigenicity in non–small cell lung cancer (NSCLC) [1,2]. One of the most consistent histological features of cancer cell invasion is the changes in tumor stroma recognized as desmoplasia. Desmoplasia is characterized by the activation of stromal fibroblasts into carcinoma-associated fibroblasts (CAFs), increased matrix protein disposition, new blood vessel formation, and immune cell infiltration. Desmoplasia is associated with tumor aggressiveness, which includes tumor cell growth, invasion, and metastases, suggesting that specific cellular or ECM components of desmoplasia promote tumor progression and metastasis [3–5]. Within the tumor stroma milieu, CAFs are the major stromal components in many types of malignancies that play a crucial role in tumor development [6–11] and are potential therapeutic targets for cancer [6]. However, recent studies suggest that CAFs are heterogeneous and contain different subpopulations with distinct phenotypes and functions, which hinder their application in diagnosis and targeted therapy [12,13]. Although significant prognostic impacts of CAFs have been studied in various tumors, including breast and lung cancers, whether CAFs are associated with good or poor prognosis is contradictory in different studies [14]. These studies present encouraging proof-of-concept findings that CAFs could be exploited for prognostication; however, they also highlight the difficulties to conclusively define an "activated stroma" and to identify the individual factors involved in clinically relevant tumor-stroma interactions. Basically, although it is generally thought that CAFs promote tumor progression, targeting alpha smooth muscle actin (α-SMA)–expressing CAFs leads to disease exacerbation in cohort of pancreatic cancer patients [15] and in a mouse model of pancreatic cancer [16,17], suggesting that different fibroblast subsets may exert opposite functions in cancer progression. For example, in oral squamous cell carcinoma, two CAF subtypes have been identified that have differential tumor-promoting capability [11]. Therefore, to precisely target the cancer-promoting CAF subsets, it is necessary to identify specific markers to define these subpopulations and understand their functions.

Here we studied the biological and molecular basis of CAF heterogeneity in desmoplasia-based tumor aggressiveness. Our data demonstrated that CAFs isolated from high– and low–CAF density tumors displayed different tumor-promoting abilities, independent of their cell number, indicating that these functional differences contribute to the aggressiveness of the tumor. In summary, we provide further insights into the biological and molecular basis of CAF heterogeneity.

Materials and Methods

Supplementary Figure S1 summarizes all the methods and sample number used in each assay and is described in Supplementary data. For the rest of Materials and Methods, please refer to Supplementary data.

Histological Assessment of Desmoplasia in NSCLC Tumors

Hematoxylin and eosin (H&E) slides were prepared from formalin-fixed, paraffin-embedded tissue of surgically resected lung tumors. Tumors were classified into high desmoplasia (HD) or low desmoplasia (LD) according to histological features, mainly the percentage of desmoplastic areas (DAs) in the tumor stroma, as assessed by three trained pathologists (S. S., T. W., M. F. S. N.). The DA was defined by high density of proliferating fibroblasts possessing enlarged nuclei greater than the size of a lymphocyte. The estimated DA was used as a proxy for characterizing HD or LD: if the DA occupied 50% or more of the tumor stroma, the tumor was considered HD. Conversely, those with <50% DA were classified as LD. These criteria were used to assess desmoplasia in 165 tumors (initially based on 169 tumors; 4 were excluded due to lack of patient information on recurrence) from UHN non-small cell lung cancer (NSCLC) patients on whom we have previously conducted microarray gene expression profiling [18], as well as 28 NSCLC tumor samples and their corresponding normal lung prior to extracting and culturing primary CAFs (CAF cohort) and normal fibroblast (NF) cells, respectively. Desmoplasia scoring on 28 tumors (primary human lung cancer) that were used to establish CAF and their corresponding NF cultured cells were further validated in the corresponding surgical slides. Desmoplasia was tested utilizing the percent stroma in the tissue as the weight in the analysis. Initial independent scores from two pathologists resulted in 77% and 86% agreement in the UHN cohort (n = 165) and the CAF cohort (n = 28), respectively; the discrepant cases were discussed, and a desmoplasia classification was achieved.

Isolation and Primary Culture of Fibroblasts

The study was conducted using a protocol approved by the Institutional Research Ethics Board. The tumor and matched normal lung tissue (at least 5 cm away from tumor) from 28 resected NSCLC specimens were harvested within 30 minutes after surgical resection, and they were used to establish cultured CAF and corresponding NF cell lines, respectively, as previously described [1]. Sampled tissues were placed in Dulbecco's modified Eagle medium (DMEM) supplemented with 10% fetal bovine serum (FBS) and antibiotics (Invitrogen, Mississauga, ON) for immediate transportation on ice to the laboratory. Tissues were minced into small pieces and digested for 1 hour at 37°C in DMEM containing 10% FBS and 0.4 mg/ml collagenase type I (Worthington Biochemical, Lakewood, NJ). The cell suspension was centrifuged at 180×g for 5 minutes, and the pellet was resuspended in the fresh DMEM containing 10% FBS and plated onto 100-mm tissue culture plates. Based on this protocol, we were able to establish 28 CAF and their corresponding NF primary culture cells. All CAF primary cultured cells were used at early passage. We maintained all CAF/NF cell lines at early passage (passage 2-5).

Tissue sections from the 28 CAF specimens were formalin-fixed and paraffin-embedded for histologic evaluation of desmoplasia. H&E staining of paraffin-embedded NSCLC tumor tissues was scanned using ScanScope AT2 (Leica Biosystems, Buffalo Groove, IL) at 20× (~0.5 μm/pixel).

Collagen Gel Contraction

This assay was performed as previously described [19]. Contraction of collagen was performed in 96-well plate. The plates were coated with sterile filtered 2% BSA in PBS (225 μl/well), incubated at 37°C overnight, and then washed three times with sterile PBS before use (250 μl/well). Fibroblasts were trypsinized, washed three times with serum free DMEM, and diluted to the cell suspension of 1×10^6 cells/ml. The cell suspension was mixed on ice with collagen solution [5 parts 2× DMEM, 1 part 0.2 M Hepes, and 4 parts collagen I (Advanced Biomatrix, San Diego, CA; 3.1 mg/ml)] at a ratio of 1:9, yielding a final concentration of 1×10^5 cells/ml and 1.2 mg/ml of collagen. A total of 100 μl collagen/cell suspension was added to each

well without introducing air bubbles. The plate was immediately incubated at 37°C to allow gels to form. After 1 hour, 100 μl DMEM was added to each well to float the gel. The plate was then incubated at 37°C for the desired time periods (after 2, 5, 8, and 24 hours). The contraction process was measured by analyzing the diameters under an inverted microscope with an ocular micrometer. Twenty-six CAFs and 23 NFs with multiple replicates were evaluated in gel assessed by the size of the diameter measured at baseline and then at 2, 5, 8, and 24 hours. One sample had 6 replicates, 4 samples had 7 replicates, 7 samples had 8 replicates, 28 samples had 9 replicates, and 9 samples had 12 replicates.

Invasion and Migration Assay

Tumor cell invasion was assessed *in vitro* by the reconstituted basement membrane (Matrigel) invasion assay, which was performed using 8-μm polycarbonate filters coated with reconstituted basement membrane (Matrigel; BD Biosciences) as previously described [1]. Prior to coating, Matrigel was diluted with cold distilled water, and 14 μg in 60 μl was added to each filter. The coated filters were dried overnight and equilibrated with serum-free RPMI for 2 hours. The medium was then removed, and the filters were placed in 24-well plates. To measure the migratory ability of A549 tumor cells, we used noncoated filters. Following this, to each filter, 5×10^4 A549 NSCLC tumor cells were added in 100 μl of RPMI containing 0.2% BSA for a 48-hour incubation at 37°C in a humidified 5% CO_2 incubator. For co-culture assays, 5×10^4 HD-CAFs ($n = 2$) and LD-CAFs ($n = 2$) and their corresponding NFs were added to the lower chamber. To study the invasion and migratory ability of A549 tumor cells in co-culture with extreme desmoplastic CAFs, we used HD^{EX}-CAFs ($n = 3$) or LD^{EX}-CAFs ($n = 3$). At the end of the incubation period, the cells on the upper surface of the filters were removed with a cotton swab, and the filters were fixed in 0.1% glutaraldehyde and stained with 0.2% crystal violet. The number of cells that migrated to the lower side of the filter was counted with a Nikon Upright microscope (OPTIPHOT; ×100) using the Image Pro program. The whole area was counted per filter. The assay was done in triplicates.

In Vivo Tumorigenicity Assay

Severe combined immune-deficient (SCID) mice were bred on-site at the Princess Margaret Cancer Centre animal facility. All manipulations were done under sterile conditions in a laminar flow hood in accordance with protocols approved by the Princess Margaret Cancer Centre Animal Care Committee. The tumorigenicity of cell lines was tested in 6-week-old male SCID mice by subcutaneous implantation of 2×10^6 A549 cells (non–small cell lung adenocarcinoma cell line purchased from the American Type Culture Collection and cultured in RPMI 1640 medium supplemented by 10% FBS) with and without 2×10^6 HD-CAFs or LD-CAFs into the abdominal flanks of the mice. In order to explore the difference of tumor-promoting potentials between HD-CAFs and LD-CAFs, four HD-CAFs and four LD-CAFs were selected. The corresponding NFs and A549 alone was used as controls. Five mice were used for each experimental group. Tumor volume was calculated as (length × width^2) × $\pi/6$.

3D Matrix Invasion Assay

A549 tumor cell line was stably transfected with a retrovirus harboring dsred tag ($A549^{dsred}$) and cultured as homospheroid and as heterospheroid with HD^{EX}-CAFs ($n = 3$) or LD^{EX}-CAFs ($n = 3$) [20] using the Nunclon Sphera plate (VWR, Mississauga, ON). Either tumor cells or fibroblasts were diluted to 1×10^6 cells/ml, and a ratio of 1:4 (tumor cells:fibroblasts) was used for making heterospheroids. Briefly, confluent monolayers were trypsinized, resuspended as single cells in RPMI +10% FBS ($A549^{dsred}$ cells) or DMEM +10% FBS, and plated in drop of 40 μl per well of 96-well Sphera plate. Cells began to form spheroids after 1 day [20]. On day 2, the spheroids were flushed in collagen type I gel and were visualized under Zeiss LSM700 confocal fluorescent microscope (Zeiss, Toronto, ON) using 5 × 0.25 NA objective at day 2 postembedding. The 3D matrix invasion areas were analyzed using texture analysis available as a plugin for the freeware Image J analysis software (http://imagej.nih.gov/ij/index.html) to evaluate the pixels in different directions around the spheroid, which is a measure of invading area.

RNA Extraction from Collagen Gel-Embedded CAFs

Cells (1×10^5) at passage 2 were seeded in 500 μl 3-D collagen type I gel matrix [5 parts 2× DMEM, 1 part 0.2 M Hepes, and 4 parts collagen type I (Advanced Biomatrix, San Diego, CA)] at a concentration of 3.1 mg/ml in a 24-well plate. After 24 hours, 1 ml of Trizol (Invitrogen, Mississauga, ON) was added to each well, and the gel was homogenized with a 1000-μl pipette.

Reverse-Transcriptase/Quantitative Polymerase Chain Reaction (RT-qPCR) Expression Profiling

Total RNA (2 μg) was reverse-transcribed using Superscript II reverse transcriptase (Invitrogen, Mississauga, ON). A 10-ng equivalent of complementary DNA was used for each qPCR assay, performed with the Stratagene Mx3000p Sequence Detection System using SYBR green 2× master mix (Stratagene, La Jolla, CA). Intron-spanning primers were designed using the Primer Express software (Perkin-Elmer Applied Biosystems, Foster City, CA). For validation of microarray expression, primers were designed based microarray probe sets using primer blast. Absolute mRNA expression and calculation for copy number gene expression were based on standard curve for each gene using control human normal lung genomic DNA. Primer sequences for *ST8SIA2* gene expression were designed based on Affymetrix-specific probe set: (forward) 5′-CCAG-TACAGGAGTATGCCCG and (reverse) 5′-TGGCATTGAC-CAAGTCCTCA. The values were normalized using housekeeping genes (RPS13 and B2M when indicated).

Microarray Gene Expression Profiling

The gene expression was obtained in extreme desmoplastic CAFs (four HD^{EX}-CAFs and four LD^{EX}-CAFs; one HD^{EX}-CAF went to senescence and was excluded from gene expression analysis). Early passage (passage 2) cultures of the 7 CAFs were embedded in collagen gel for 24 hours, and total RNA was isolated as described previously [21]. The gene expression microarray profiling was performed by the Princess Margaret Genomics Centre (https://www.pmgenomics.ca/pmgenomics/) using the Illumina Human HT-12v4 DASL microarray platform. The raw data from BeadChips (seven samples passed Illumina sample-dependent and -independent quality controls matrices) were preprocessed using BeadArray specific method (R package lumi v3.) for Illumina microarray [22]. The signal intensities were log2 transformed, background corrected, and normalized using robust spline normalized method. The signals were then filtered using the probe signal detection threshold ($P < .05$). Expression values were summarized at the gene-core/whole-transcript level based on

HT12v4 annotation library. Preprocessed data are available through the Gene Expression Omnibus database (https://www.ncbi.nlm.nih.gov/geo/query/acc.cgi?acc=GSE116679).

Differentially expressed genes between HD-CAFs and LD-CAFs were identified by robust linear model analysis (fold change ≥1.5; adjusted P value < .1, R package).

Western Blot Analysis

The experimental procedure is described in Supplementary data.

Stable Transfection of Polysialyltransferase (ST8SIA2) Construct into CAFs Primary Cultured Cells

Lentiviral vector carrying *ST8SIAII* (pLenti-GIII-CMV-ST8SIA2) for overexpressing ST8SIA2 in HD-CAF and the control vector (pLenti-GIII-CMV-GFP) were purchased from ABM (Richmond, BC). ORF expression clone for *ST8SIAII* (EX-U0376-Lv122) for overexpressing *ST8SIAII* in LD-CAF and empty control vector (pReceiver-Lv122 (EX-NEG-lV122)) were purchased from GeneCopoeia (Rockville, MD). Lentiviruses were prepared as described [1] by transfecting three plasmids into 293T cells: 1) pMDLg/pRRE, the vesicular stomatitis virus (VSV-G) envelope plasmid pCMV-VSG; 2) the rev-expressing plasmid pRSV-Rev; and 3) one of either of the gene transfer vector pLenti-GIII-CMV-ST8SIA2 or the empty control pLenti-GIII-CMV-GFP vector. Stocks were stored frozen at −80°C. Early passage cultures of HD^{EX}-CAFs were infected with the ST8SIA2 lentivirus or empty control lentivirus.

Stable knockdown of *ST8SIAII* gene expression in HD-CAF was established using lentiviral- shRNA vector (plentiLox; PLL 3.7. ST8SIA2 shRNA). As control, we used lentiviral- shRNA vector expressing *GFP* (plentiLox; PLL 3.7.GFP shRNA). The stably transfected cells were selected using 1 μg/ml puromycin.

Statistical Analysis

Differences in tumor growth rates of xenografts between HD-CAFs and LD-CAFs and NFs were tested using linear mixed-effects model. To stabilize the residuals, a square root transformation was applied to the tumor volume. The differences in migration, invasion, and mRNA expression between HD and LD were tested by Mann-Whitney test. The Wilcoxon signed rank test was utilized for the comparison between CAFs and NFs for their gel contraction activity. For the association between the desmoplasia and the relapse rate (RR), the time to event was calculated as the duration between surgery and either relapse or death or last-follow-up. The occurrence of relapse was the event for RR. The deaths in the absence of relapses were considered competing risk. The probability of relapse was calculated with the competing risks specific techniques (cmprsk package in R 3.2.2), i.e., the estimation of the probability of relapse was based on the cumulative incidence function, and the adjusted effect of desmoplasia on relapse was tested utilizing the Fine and Gray model. Since in the UHN cohort the desmoplasia was assessed in the tumor and not necessarily in only stroma, the analysis was weighted for the amount of stroma in the tumor tissue for each patient.

Results

Clinical Impact of Desmoplasia on NSCLC Prognosis

We first investigated whether high CAF content was indeed associated with more aggressive tumors. Tumors were classified into HD or LD according to histological features, mainly the percentage of DAs in the tumor stroma. The DA was defined by high proliferation of fibroblasts. The estimated DA was used as a proxy for characterizing HD or LD (Figure 1). Two pathologists assessed the degree of desmoplasia in representative tumor sections of 165 NSCLC patients (UHN cohort) who had undergone curative resection. Using their consensus scores, 61 tumors (37%) were classified as HD and 104 (63%) as LD (Figure 2, *A* and *B*; Supplementary Table S1). Desmoplasia was associated with the risk for relapse in this patient cohort. The patients with HD tumors had significantly higher RR than those with LD tumors (HR = 2.45; P value = .011) (Figure 2*C*). The prognostic impact of desmoplasia remained significant when the model was adjusted for age, sex, stage, and tumor histology (HR = 2.47, P = .027) (Table 1). This association was stronger among adenocarcinoma patients. The patients with HD had poor outcome in comparison to the patients with LD (HR = 4.01, P = .00064, Figure 2*D*). The desmoplasia characteristic remained significant when the effect was adjusted for age, sex, and stage (HR = 3.69, P = .004) (Table 1).

To determine whether CAF density or CAF functional heterogeneity contributes to the aggressiveness of the tumor, we isolated CAFs from 28 NSCLC resected tumors. Using the same predefined criteria, desmoplasia was assessed in 28 NSCLC tumor samples prior to extracting and culturing primary CAF cells (CAF cohort) (Supplementary Table S2). Most tumors (23/28; 82.14%) were diagnosed as adenocarcinoma. Fifteen samples were classified as HD tumors and 13 as LD tumors. To avoid heterogeneity issues associated with sampling, the histologic review and DA scores on these tumors (26/28) were validated in multiple tumor regions from corresponding surgical pathology specimens except one tumor, which was classified as LD in the surgical slide and as HD in CAF cohort (Supplementary Table S3).

To confirm the absence of chromosomal variations in primary fibroblasts cell cultures (CAFS and their matched NFs), we performed Shallow WGS-CNV sequencing to analyze copy number variation. We showed that CAF and corresponding NF primary cell cultures are diploid compared to the three randomly selected established human tumor cell lines (Supplementary Figure S2).

CAF-Specific Markers in HD- and LD-CAFs

Since in our previous studies α-SMA and integrin α11 were both recognized as important markers of CAFs in lung cancer [1,21], we asked whether HD- and LD-CAFs could be characterized depending on these markers. These two markers were assessed by Western blot analysis on the 23 cultured CAF and NF primary cultured cells. The expression of integrin α11 and α-SMA was significantly higher in CAF compared to their corresponding NF primary cultured cells (Supplementary Figure S3, *A* and *B*; Supplementary Table S5). We also observed a significant correlation between α-SMA and integrin α11 protein levels in CAFs (r = 0.63; P = .0013) (Supplementary Figure S3*C*; Supplementary Table S4) as well as in NFs (r = 0.61; P = .0019) (Supplementary Figure S3*D*; Supplementary Table S4). Although we observed a significant difference between CAFs and NFs at the protein levels for both integrin α11 and α-SMA (P = .0002 and P = .0018, respectively), the differences between HD-CAFs and LD-CAFs were not statistically significant (Supplementary Table S5).

Using RT-qPCR, we further evaluated in 26 desmoplastic CAF primary cultured cells the expression of 11 genes that made up our previously published CAF prognostic gene signature [1] (for primers list, please refer to Supplementary Table S6). The mRNA expressions of 6 out of the 11 genes (*B3GALT2*, *OXTR*, *PDE3B*, *CLU*,

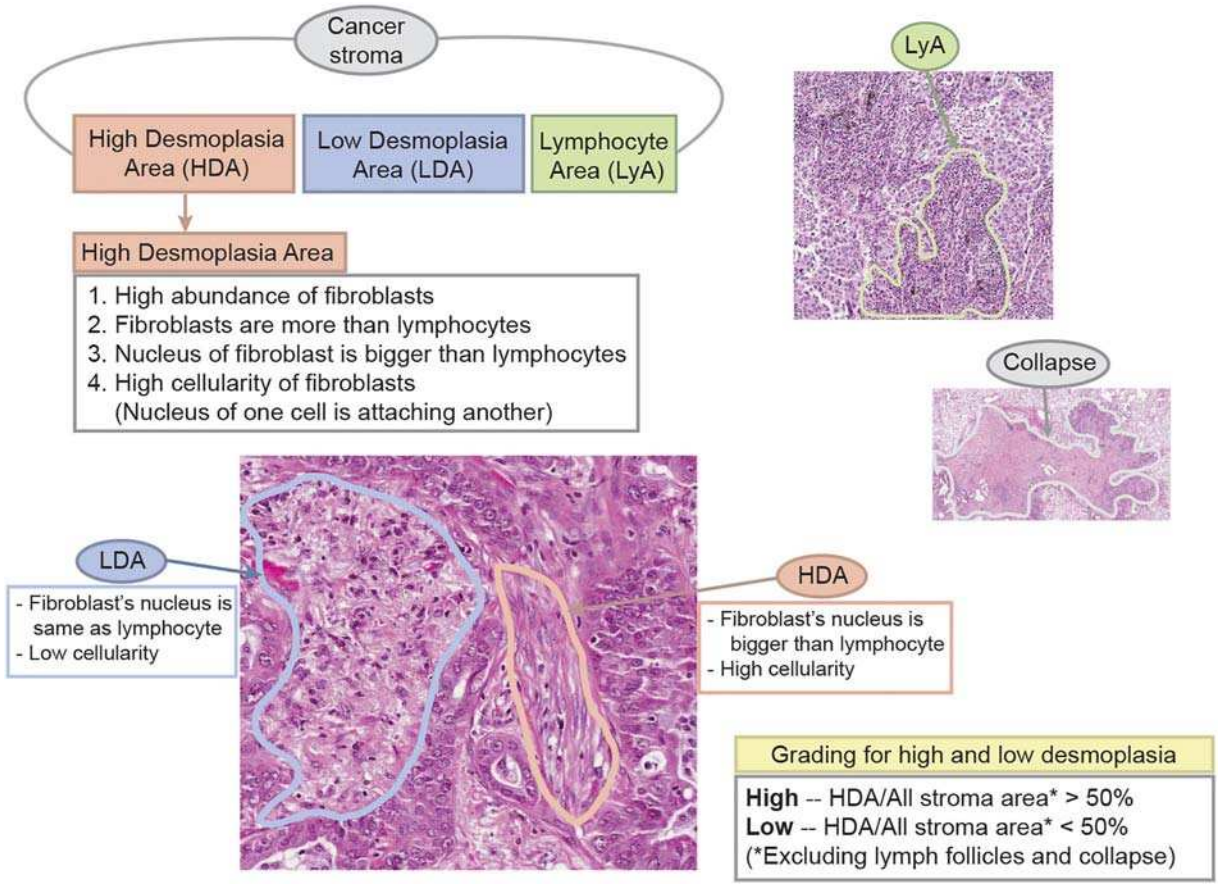

Figure 1. Definition of desmoplasia. H&E slides were prepared from formalin-fixed, paraffin-embedded tissue of surgically resected lung tumors. Each tumor sample was graded as HD or LD based on the percentage of DAs in total tumor stroma, as assessed by two pathologists. The high–desmoplasia area (HDA) stroma is defined by the following characteristics: a high density of fibroblasts with minimal intervening mature collagen, and fibroblasts possessing enlarged nuclei greater than the size of a lymphocyte. If the stromal HDA occupies 50% or more of the tumor stromal area, the tumor is considered to have HD. Conversely, those with <50% HDA are classified as LD.

COL14A1, and *GAL*) were significantly different between CAFs and NFs, validating the findings of our earlier study [1] (Supplementary Table S7). These results remained significant after a Bonferroni adjustment for multiple testing was applied. Of these six genes, two were upregulated in CAFs (*B3GALT2* and *OXTR*) and four were downregulated in CAFs (*PDE3B*, *CLU*, *COL14A1*, and *GAL*) (Supplementary Table S7). However, none of the 11 prognostic genes showed statistical significant difference between HD-CAFs and LD-CAFs (Supplementary Table S7).

HD-CAFs Enhance Collagen Matrix Remodeling and Tumorigenicity of NSCLC cells

We aimed to determine whether the desmoplasia-associated poor prognosis was due to CAF density only or to differences in desmoplastic CAF functions. We first evaluated the ability of primary cultured CAFs to remodel collagen matrix (*in vitro* recognized as collagen gel contraction), which has been shown to affect tumor invasion and growth [2]. We showed that HD-CAFs had significantly higher collagen gel contraction activity compared to LD-CAFs (Figure 3*A*, Supplementary Table S8). Also, we showed that LD-CAFs behaved the same as NFs, and both were different from HD-CAFs. We then measured ability of desmoplastic CAFs in promoting tumor cell invasion. We selected two HD-CAF and two LD-CAF primary cultured cells and their matching NFs based on their level of collagen gel contraction. Using *in vitro* Transwell Matrigel invasion assay, we observed increased invasion of A549 tumor cells into Matrigel in co-culture with HD-CAFs but not with LD-CAFs or A549 tumor cells alone (Figure 3*B* and Supplementary Table S9). Furthermore, *in vitro* co-culture migration assay showed increased migration of A549 tumor cells in co-culture with HD-CAFs but not with LD-CAFs or alone (Figure 3*B* and Supplementary Table S9). To confirm aggressiveness of high desmoplastic CAFs, we did an *in vivo* tumor growth assay. In addition to selected CAFs used in *in vitro* invasion and migration assay, we included two HD-CAF and two LD-CAF primary cultured cells and their matching NFs based on collagen remodeling. Both HD- and LD-CAF cells were separately co-injected subcutaneously with A549 tumor cells into SCID mice. The tumor growth rate for all *in vivo* tumor-promoting curves of eight pairs of CAFs and NFs co-injected with A549 tumor cells including A549 tumor cell alone as control was analyzed using the mixed-effect model. The tumor growth rate in the HD-CAFs/A549 was significantly higher than in LD-CAFs/A549 and NFs/A549 ($P < .0001$; Supplementary Table S10), but there was no statistical difference between LD-CAFs/A549 versus NF/A549 ($P = .66$; Figure 3*C*). We did not observe any tumor growth when we injected HD-CAFs, LD-CAFs, or NFs alone. We observed the slowest tumor growth rate in tumor from injecting A549 tumor cells alone. This implies that the increased tumor growth rate observed in HD-CAFs/

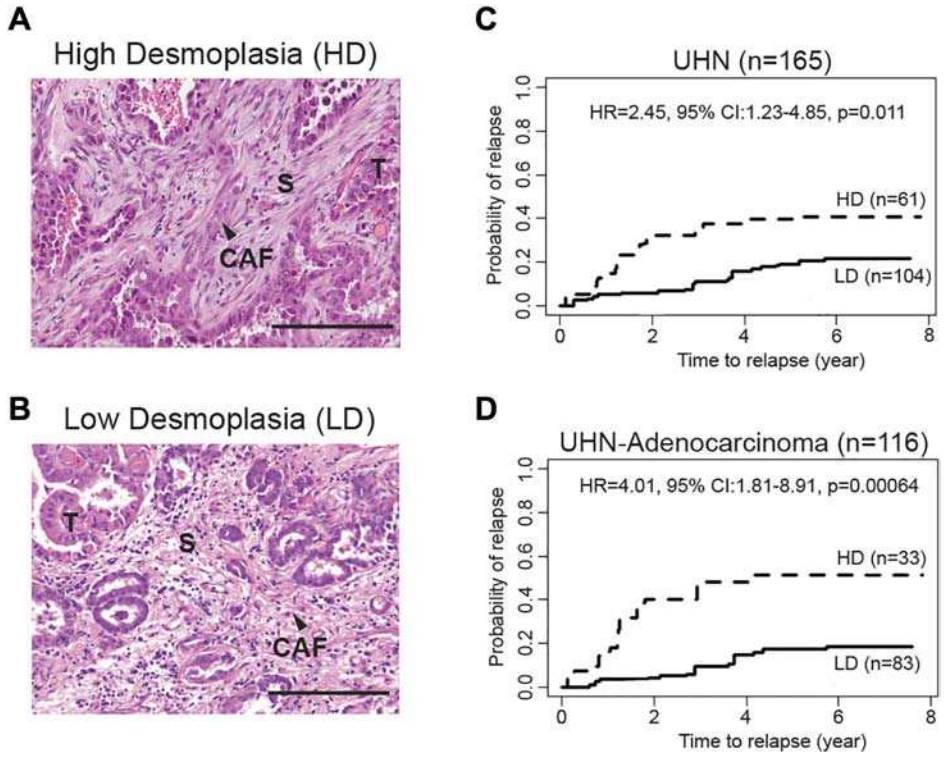

Figure 2. The association between desmoplasia and the RR was tested for 165 patients. (A and B) The criteria for desmoplasia as described in Figure 1 were used to assess desmoplasia in 165 tumors from UHN NSCLC patients. (C) The RR was estimated using the cumulative incidence function, and the comparison between 165 HD and LD tumors was performed using Wald test within the Fine and Gray model. (D) The association between desmoplasia and the RR within adenocarcinoma subgroup was tested for 116 patients. The RR was estimated using the cumulative incidence function, and the comparison between HD and LD tumors was performed using Wald test within the Fine and Gray model.

A549, LD-CAFs/A549, and NFs/A549 was due to the promoting ability of fibroblasts. These data indicated that high level of desmoplasia is associated with tumor aggressiveness, independent of the CAF number, thus suggesting that the aggressiveness of the tumor depends more on CAF function rather than CAF density.

HD^{EX}-CAFs Enhance Invasion of NSCLC Tumor Cells

We then aimed to understand the molecular mechanisms of high desmoplastic CAFs in tumor aggressiveness. We focused on collagen matrix remodeling where differences in gel contraction between HD- and LD-CAFs indicated that they are behaving in a functionally different manner. Therefore, HD-CAFs and LD-CAFs were clustered based on their correlation between collagen matrix remodeling activity (collagen gel contraction) and desmoplasia (Supplementary Figure S4). We noticed an overlap of HD-CAFs and LD-CAFs when the DA score ranged from 20% to 60%. Therefore, we selected three extreme HD-CAFs (HD^{EX}-CAFs; desmoplasia >60% and collagen gel diameter < median) and four extreme LD-CAFs (LD^{EX}-CAFs; desmoplasia <20% and collagen gel diameter > median) to better define CAF subgroups for functional analysis. *In vitro* 3D collagen matrix invasion assay showed increased invasion of A549^{dsRed} tumor cells into collagen type I in heterospheroid culture with HD^{EX}-CAFs but not with LD^{EX}-CAFs or as monospheroid of A549^{dsred} tumor cells isolated (Figure 3, *D* and *E* and Supplementary Table S11). Using *in vitro* co-culture Matrigel invasion assay, we observed increased invasion of A549 tumor cells into Matrigel in co-culture with HD^{EX}-CAFs but not with LD^{EX}-CAFs or A549 tumor cells alone (Figure 3*F* and Supplementary Table S12). Furthermore, *in vitro* co-culture migration assay showed increased migration of A549 tumor cells in co-culture with HD^{EX}-CAFs but not with LD-^{EX}-CAFs or alone (Figure 3*F* and Supplementary Table S12).

Table 1. The Effect of Desmoplasia on Clinical Outcome

	UHN (n = 165)			UHN-Adenocarcinoma (n = 116)		
	HR	95% CI	*P* Value	HR	95% CI	*P* Value
Age (≥65 vs. <65)	1.16	0.48-2.77	.74	1.01	0.34-3.03	.98
Sex (M vs. F)	1.58	0.74-3.38	.24	1.11	0.45-2.74	.83
Stage (II vs. I)	1.54	0.72-3.29	.27	1.39	0.53-3.61	.5
Histology (Ade vs. other)	1.59	0.69-3.69	.28			
Desmoplasia (HD vs. LD)	2.47	1.11-5.53	.027	3.69	1.52-8.98	.004

RR was adjusted for clinical factors in the UHN cohort and adenocarcinoma patient subgroup when the model was weighted for the amount of stroma. The Fine and Gray model was utilized. *Ade*, adenocarcinoma.

Gene-Expression Profile of HD-CAFs in NSCLC

To evaluate genes that are involved in tumor aggressiveness of high desmoplastic CAFs, differential gene expression analysis was performed. A total of 13 differentially expressed genes (nine upregulated and four downregulated) were identified (fold change > 1.5; adjusted *P* value < .1) between HD^{EX}-CAFs and LD^{EX}-CAFs (accession no. GSE116679) (Figure 4*A*; Supplementary Table S13). The genes with fold change expression ≥2 and ≤−2 were selected for validation (Figure 4*B*). Using RT-qPCR, we validated four

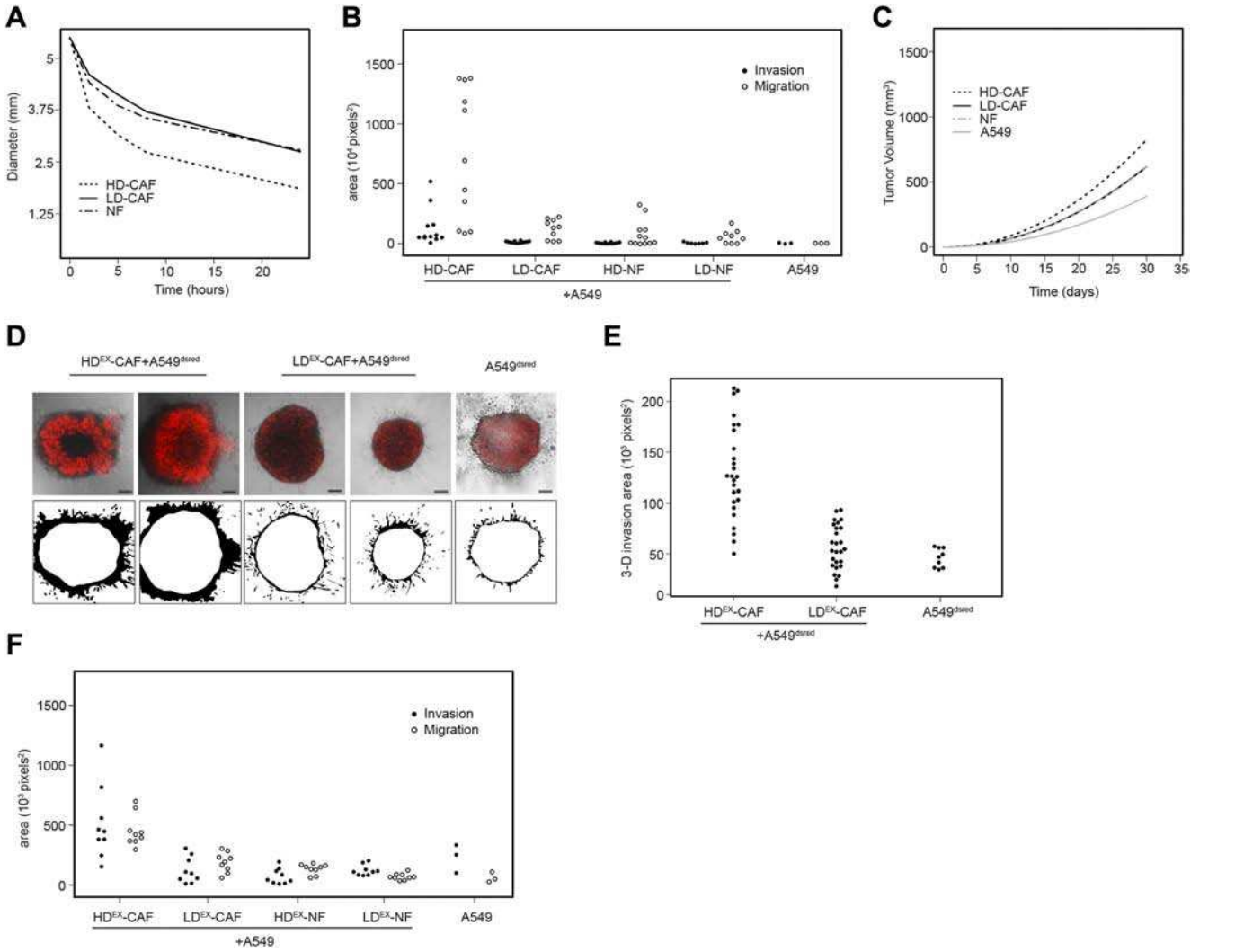

Figure 3. Desmoplasia-related CAF heterogeneity influences collagen matrix remodeling and tumor cell growth and dissemination. (A) The collagen gel contraction estimates at each time point for LD-CAFs, HD-CAFs, and their corresponding NFs. The lines represent the averages of the diameters per group and at each specific time point. The comparisons between groups at each time point were performed utilizing the Wilcoxon signed rank test. (B) *In vitro* Transwell assay measuring the invasion and migration ability of A549 tumor cells in co-culture with HD-CAFs or LD-CAFs. Quantification has been performed using the Image Pro program. Statistic tables for each data are provided in Supplementary data. (C) HD-CAFs, LD-CAFs, and NFs were individually mixed with A549 tumor cells and were co-injected subcutaneously in SCID mice. The graph shows the predicted tumor growth across the groups (81 mice) and analyzed based on mixed-effect model. The significance is analyzed using the mixed-effect model. (D) Heterospheroids of HD^{EX}-CAFs + $A549^{dsred}$ or LD^{EX}-CAFs + $A549^{dsred}$ as well as monospheroid of $A549^{dsred}$ cells were embedded in collagen gel, and the invasion into the collagen type I gel were visualized for 2 days using confocal microscopy. Scale bars: 200 μm. (E) Quantification of the $A549^{dsred}$ tumor cell invading area measured by image J. (F) *In vitro* Transwell assay measuring the invasion and (G) migration ability of A549 tumor cells co-culture with HD^{EX}-CAFs or LD^{EX}-CAFs. Quantification has been performed using the Image Pro program. Statistical analysis for each data is provided in Supplementary data (Supplementary Table S8-12).

significantly upregulated genes (*ST8SIA2*, *WNT7B*, *SLITRK6*, and *IGFL3*) (Figure 4*C*; for primers list, please refer to Supplementary Table S14). RT-qPCR failed to validate the gene expression of *HEPH* and *SCML1* (Figure 4*C* and Supplementary Table S15).

To be consistent with our selection of extreme desmoplasia cases in CAF cohort, we subgrouped 165 NSCLC patients in UHN clinical cohort to extreme desmoplasia cases (HD^{EX}-UHN cohort; desmoplasia >60% and LD^{EX}-UHN cohort; desmoplasia <20%). RT-qPCR analysis using Affymetrix probe set-specific primers showed that the most top upregulated differentially expressed gene, *ST8SIA2,* has significant increase in copy number gene expression (P value = .026) in HD^{EX}-UHN cohort compared to LD^{EX}-UHN cohort (Figure 4*D* and Supplementary Table S16).

ST8SIA2 Enhances the Invasion of NSCLC Tumor Cells

To investigate the function of ST8SIA2 in tumor aggressiveness, we first confirmed ST8SIA2 protein expression in three HD^{EX}-CAFs compared to three LD^{EX}-CAFs (Figure 5, *A* and *B*, Supplementary Table S17, P = 7.396e-07). We transfected two different ST8SIA2 shRNAs in HD^{EX}-CAF (shST8SIA2#1 and shST8SIA2#2), displaying 73% and 33% of ST8SIA2 expression inhibition, respectively (Figure 5*C* and Supplementary Table S18). Knockdown of 70% of

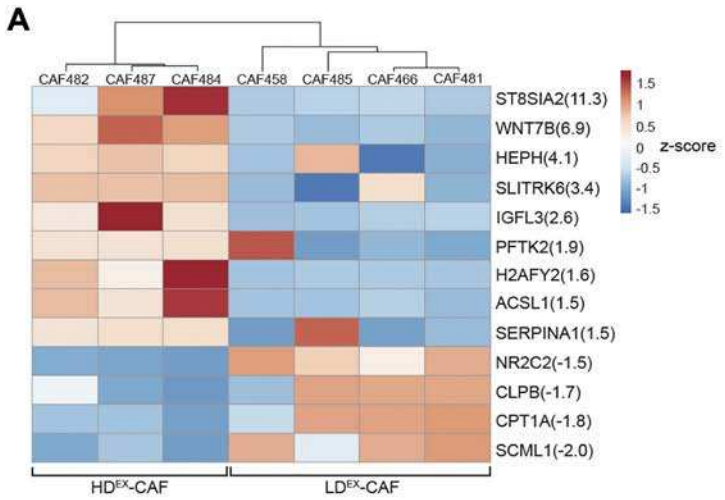

B

Gene Symbol	Description	Fold Change	p value	adj. p value
Differentially up-regulated genes in HD^{EX}-CAF				
ST8SIA2	ST8 alpha-N-acetyl-neuraminide alpha-2,8-sialyltransferase 2	11.3	7.9e-06	0.021
WNT7B	wingless-type MMTV integration site family, member 7B	6.9	3.8e-05	0.046
HEPH	hephaestin	4.1	1.4e-04	0.093
SLITRK6	SLIT and NTRK-like family member 6	3.4	2.8e-07	0.002
IGFL3	IGF-like family member 3	2.6	1.2e-04	0.087
Differentially down-regulated genes in HD^{EX}-CAF				
SCML1	sex comb on midleg-like 1 (Drosophila)	-2.0	1.4e-04	0.093

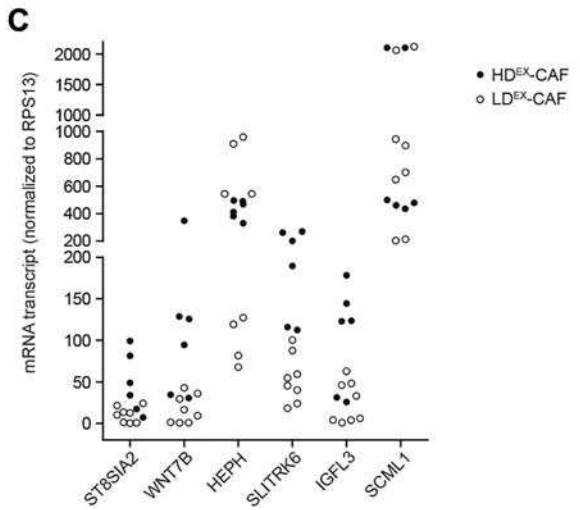

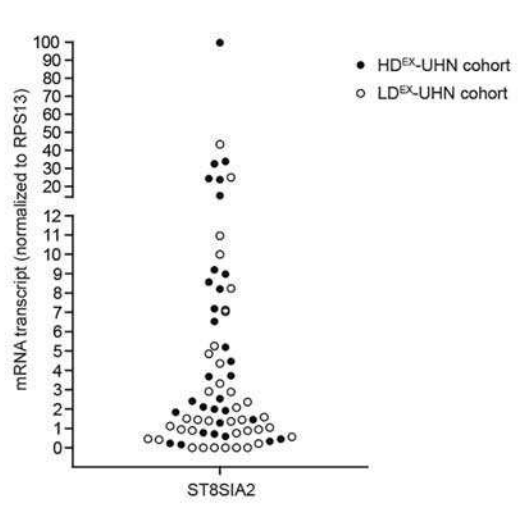

Figure 4. Differential gene expressions in HD^{EX}-CAFs versus LD^{EX}-CAFs. (A) Heat map of 13 differential gene expressions between HD^{EX}-CAFs and LD^{EX}-CAFs. Pearson's correlation coefficients between all samples were calculated based on 13 differential gene expressions between HD^{EX}-CAFs and LD^{EX}-CAFs. Agglomerative hierarchical clustering was performed using these correlation coefficients as the distance metric and complete linkage. Rows correspond to individual genes, and columns correspond to individual samples. (B) Five upregulated (fold change ≥ 2; adjusted P value $< .1$) and one downregulated (fold change ≤ -2; adjusted P value $< .1$) expression genes in HD^{EX}-CAFs versus LD^{EX}-CAFs were selected for RT-qPCR analysis. (C) Differential gene expressions in Microarray analysis were validated by absolute RT-qPCR using mRNA from three HD^{EX}-CAF and four LD^{EX}-CAF primary cultured cells. (D) Using RT-qPCR, the difference for the top upregulated differential gene expression (*ST8SIA2*) in extreme desmoplastic tumors in UHN clinical cohort (HD^{EX}-UHN cohort and LD^{EX}-UHN cohort) was calculated, and statistic was performed using Mann-Whitney test. The values were normalized using the housekeeping gene *RPS13*. Absolute mRNA expression was based on standard curve for each gene using control normal human lung genomic DNA. Statistical analysis for each data is provided in Supplementary data (Supplementary Table S15 and 16).

ST8SIA2 gene expression in HD^{EX}-$CAF^{shST8SIA2\#1}$ resulted in a significant inhibition of $A549^{dsred}$ tumor cells invasion into collagen type I in heterospheroid cultures (Figure 5*D* and Supplementary Table S19, $P = .0022$). Inhibition of *ST8SIA2* gene expression by 30% in HD^{EX}-$CAF^{shST8SIA2\#2}$ also showed a decrease in $A549^{dsred}$ tumor cells invasion that however was not significant. In parallel, stable overexpression of ST8SIA2 in HD^{EX}-$CAF^{ST8SIA2}$ (Figure 5*E*) showed a significant increase in invasion of $A549^{dsred}$ tumor cells into 3D collagen type I matrix compared to corresponding control GFP transfected HD^{EX}-CAF (HD^{EX}-CAF^{GFP}) (Figure 5*F* and Supplementary Table S19, $P = .0042$). We then overexpressed ST8SIA2 in LD^{EX}-CAF (LD^{EX}-$CAF^{ST8SIA2}$) to determine if we can rescue the A549 tumor cell invasive phenotype similar to what we showed using HD^{EX}-CAF (Figure 5*G*). LD^{EX}-$CAF^{ST8SIA2}$ enhanced invasive ability of A549 in 3D collagen matrix compared to control LD^{EX}-CAF^{GFP} (Figure 5*H* and Supplementary Table S19, $P = .0152$), indicating that ST8SIA2 expression is important in promoting NSCLC invasion.

Clinical Impact of ST8SIA2 on NSCLC Prognosis

We explored the prognostic properties and clinical relevance of ST8SIA2 by using NSCLC microarray gene expression datasets. We analyzed the association of *ST8SIA2* gene expression with the risk of relapse in UHN clinical cohort (GSE50081). Our finding showed that *ST8SIA2* is significantly prognostic for rate of relapse using both UHN cohort microarray data (Affymetrix) (P value = .033) and RT-qPCR gene expression data (P value = .0027) in extreme desmoplastic tumors in UHN cohort (Table 2). We further validated *ST8SIA2* as prognostic gene associated with the risk of relapse in two additional independent NSCLC clinical datasets from DCC (GSE68465) (P value = .00032) and Okayama (GSE31210) (P value = .005) (Supplementary Tables S20 and S21).

Discussion

Desmoplastic tumor stroma is mainly characterized by abundance of proliferating CAFs particularly at the boundaries between the invasive cancer and the host tissue. Desmoplasia is associated with enhanced tumor cell invasiveness and has been associated with tumor cell malignancy [23–25]. However, there are studies suggesting that ablation of desmoplasia renders tumors more aggressive [16,17]. These conflicting effects of desmoplasia suggest that functions of CAFs are not fully understood.

We have demonstrated that activated cancer stroma characterized as high desmoplasia has prognostic significance in NSCLC patients. Other groups have reached this statement in the past [26,27], but their definition of desmoplasia was different, integrating more the collagen aspect rather than fibroblast density as we did in this study. Furthermore, we demonstrated that functional heterogeneity of desmoplastic CAF is a determinant factor of NSCLC aggressiveness. Here, we showed that compared to LD-NSCLC tumors, CAFs resected from HD-NSCLC tumors demonstrated higher matrix reorganizing ability and promotion of tumor cell invasion and growth, confirming the existence of functional heterogeneity among NSCLC CAFs. We profiled significant gene expression in primary cultured CAFs after they remodeled the collagen matrix. We have identified 13 differential CAF gene expressions that were significantly correlated with desmoplasia. The top upregulated differentially expressed gene between extreme desmoplastic HD-CAFs versus LD-CAFs, *ST8SIA2,* increased invasion ability of A549 NSCLC tumor cell line when overexpressed in LD^{EX}-CAFs and increased further the invasion ability of A549 tumor cells when overexpressed in HD^{EX}-CAFs. Most of all, ST8SIA2 was prognostic for rate of relapse in UHN and two other independent clinical cohorts.

The mechanism contributing to the phenotypic and functional heterogeneity among fibroblasts remains debated in lung cancer. Only a few studies on the functional heterogeneity of CAFs in different types of cancers have been reported. The effect of CAFs on colon cancer cell migration ability identified a CAF gene expression signature. This signature was able to classify colon cancer patients into high- and low-risk groups [28]. Recently, a new functionally distinct subset of CAFs was identified that was preferentially abundant in breast chemoresistant tumors [29].

To date, the stroma influence on the tumor has mainly been described as a prognostic marker in lung, colon, and breast cancer [30,31]. Stroma-rich tumors in breast cancer patients were associated with an increased risk of relapse [31]. Our analysis of the clinical relevance of desmoplasia in a large cohort of 165 NSCLC patients showed that desmoplasia is significantly associated with patient RR. This posited the functional and clinical relevance of CAF heterogeneity in NSCLC tumors.

To understand the biological role of desmoplasia in aggressiveness of NSCLC tumors, we first characterized two CAFs subsets from 28 NSCLC patient tumors which were scored and classified based on desmoplasia. Based on our RT-qPCR analysis using a prognostic 11-gene signature of CAFs from NSCLC patients [1], we could differentiate between CAFs and their corresponding NFs; however, we were unable to differentiate between HD-CAFs and LD-CAFs. One explanation is that the 11–CAF gene signature is based on *in vitro* CAFs primary cultured cells comparing to their matched NFs and is not related to the function of CAFs. Furthermore, we investigated two CAF markers—integrin α11 and α-SMA—that are expressed in CAF from NSCLC tumors. We observed a significant correlation in mRNA expression and protein between α-SMA and integrin α11 within CAFs and NFs, but no correlation between these two markers within HD-CAFs and LD-CAFs, indicating that desmoplasia is not a mere quantification of fibroblasts but is a specific characteristic of activated stroma. Activation state of CAFs is a major hallmark of marked tumor desmoplasia. Collagen gel contraction reflects collagen matrix reorganization and is an *in vitro* measurement of CAF activation. Harris et al. [32] have suggested that traction forces at the surface of fibroblasts are the driving forces for collagen remodeling and tissue morphogenesis. A model has been proposed where the organization of the collagen meshwork explains how traction forces might act *in vivo* to organize collagen fibers [33]. Our results showed that collagen gel contraction activity of CAFs is correlated with desmoplasia. Collagen remodeling ability of CAFs is considered an independent survival prognostic factor in many cancers (2, 3). Our finding that CAF activity of collagen reorganization was closely related to their tumor-promoting effect is consistent with a previous study in CAFs from breast cancer [34]. In another study, α-SMA staining and collagen contractibility of CAFs from colon carcinoma suggested a link between the different activation level of CAFs and their ability to enhance tumorigenicity [28]. It has been speculated that CAFs share the same activation state, but their expression of activation markers, such as α-SMA, FSP1, FAP, or others, may differ [35]. Here, we present the first study that demonstrates the correlation between desmoplasia and the heterogeneous activation state of CAFs.

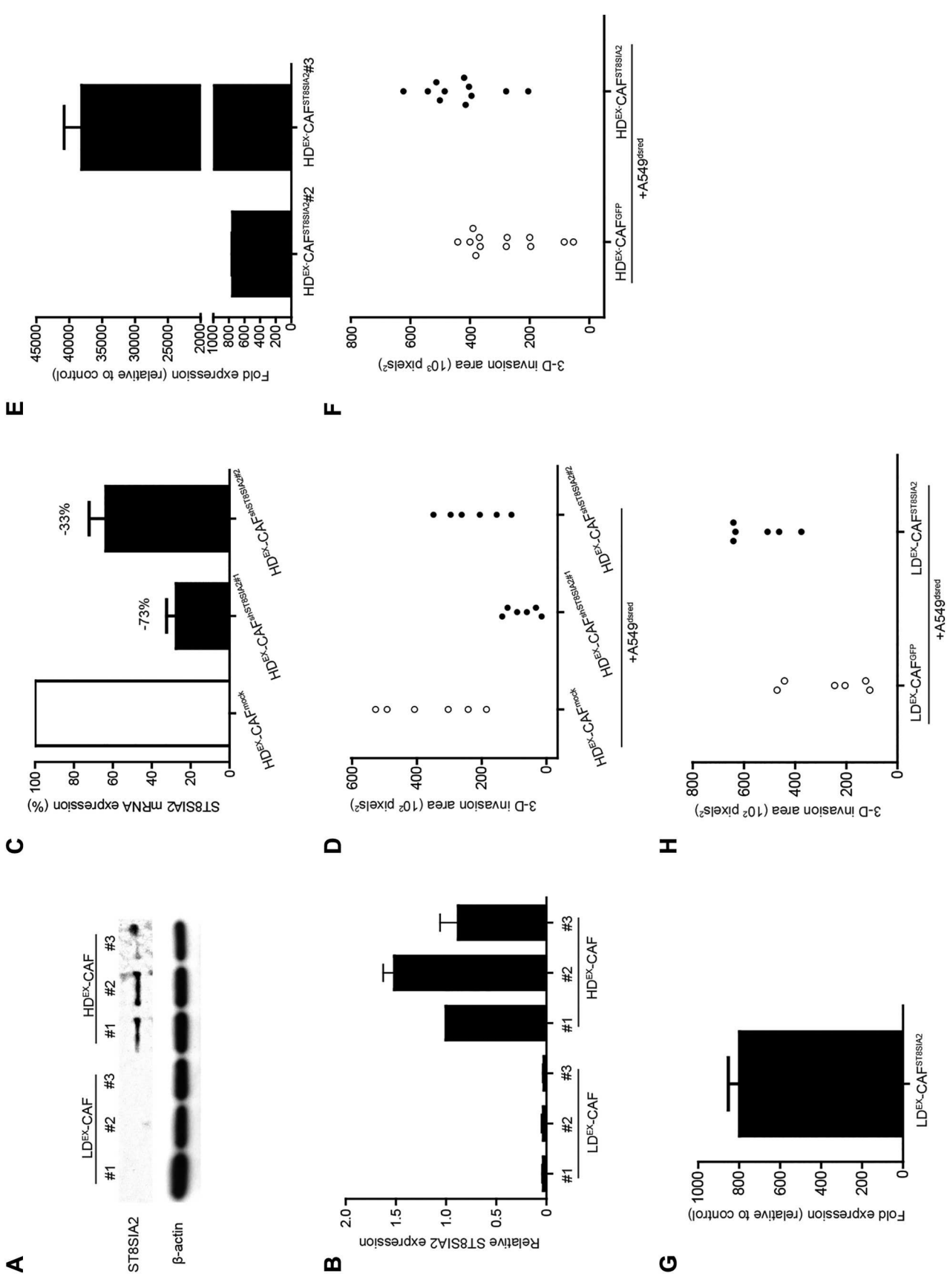
A
LDEX-CAF
#1
#2
#3
HDEX-CAF
#1
#2
#3
ST8SIA2
β-actin
B
Relative ST8SIA2 expression
2.0
1.5
1.0
0.5
0
#1
#2
#3
LDEX-CAF
#1
#2
#3
HDEX-CAF
C
ST8SIA2 mRNA expression (%)
100
80
60
40
20
0
-33%
-73%
HDEX-CAFmock
HDEX-CAFshST8SIA2#1
HDEX-CAFshST8SIA2#2
D
3-D invasion area (10² pixels²)
600
400
200
0
HDEX-CAFmock
HDEX-CAFshST8SIA2#1
HDEX-CAFshST8SIA2#2
+A549dsred
E
Fold expression (relative to control)
45000
40000
35000
30000
25000
2000
1000
800
600
400
200
0
HDEX-CAFST8SIA2#2
HDEX-CAFST8SIA2#3
F
3-D invasion area (10³ pixels²)
800
600
400
200
0
HDEX-CAFGFP
HDEX-CAFST8SIA2
+A549dsred
G
Fold expression (relative to control)
1000
800
600
400
200
0
LDEX-CAFST8SIA2
H
3-D invasion area (10² pixels²)
800
600
400
200
0
LDEX-CAFGFP
LDEX-CAFST8SIA2
+A549dsred

Table 2. Clinical Impact of *ST8SIA2* on the RR for the UHN Cohort

Data Set	*n*	Probe Set/Gene	Hazards Ratio	95% Confidence Interval	*P* Value
Affymetrix Microarray, extreme desmoplasia values	71	X221285_at /ST8SIA2	4.93	1.14-21.4	.033
qPCR, extreme desmoplasia values	69	X221285_at /ST8SIA2	1.18	1.06-1.32	.0027

The table shows the clinical impact of ST8SIA2 gene expression measured by microarray (Affymetrix) and qPCR in the UHN clinical cohort. The hazards ratios and the *P* values were calculated utilizing the Fine and Gray method for competing risks.
Two samples not present in qPCR data were excluded from microarray data. This dataset removes two patient samples from which we were not able to obtain qPCR data.

The functionality of CAFs has been demonstrated using *in vivo* studies such as co-injection of CAFs together with tumor cells, which enhances tumor growth by promoting ECM synthesis and stiffening, inducing angiogenesis, and recruiting growth-promoting inflammatory cells such as macrophages [2,7,36–38]. Our data showed that HD-CAFs promote NSCLC tumor growth compared to LD-CAFs. Furthermore, *in vitro* data using Matrigel invasion assay and 3D heterospheroid assay showed the enhanced invasive ability of tumor cells co-cultured with HD-CAFs in comparison to those co-cultured with LD-CAFs. These results suggest that HD-CAFs and LD-CAFs are functionally heterogeneous with respect to their ability to promote tumor growth and cancer cell invasion, respectively.

To characterize the phenotype of CAF activation, we profiled significant gene expression in primary cultured CAFs during collagen matrix remodeling. We have identified 13 significantly differentially expressed genes in extreme cases of HD-CAFs versus extreme cases of LD-CAFs. We showed that one of the top upregulated genes, *ST8SIA2*, was prognostic for rate of relapse in extreme cases of UHN clinical cohort and in two other independent clinical cohorts. Moreover, overexpression of ST8SIA2 in HD-CAF and LD-CAF increased A549 NSCLC tumor cell line dissemination in a 3D collagen matrix heterospheroid culture, whereas ST8SIA2 knockdown in HD-CAF decreased A549 tumor cell invasion. These results indicated the crucial role of ST8SIA2 in tumor aggressiveness. ST8SIA2 is a polysialyltransferase that synthesizes polysialic acid (PSA) chains on different substrata, including the neural cell adhesion molecule (NCAM), which once substituted with PSA has been shown to increase tumor cell migration [39]. It is interesting to note that PSA-NCAM can be shed and acts in its proximate environment [40]. It has also been reported that overexpression of ST8SIA2 can mediate tumor cell invasiveness of hepatocellular carcinoma and small cell lung cancer by regulating activity of the PI3K/Akt and FGFR pathways, respectively [41,42]. In triple-negative breast cancer models, Hedgehog ligand secreted by tumor cells activates CAFs, leading to upregulation of ST8SIA2 expression [43]. Interestingly, in the UHN dataset, we observed a correlation between ST8SIA2 and Desert hedgehog ligand (DHH) gene expression ($r = 0.504$, P value = $7.51e^{-6}$), suggesting that hedgehog signaling may in part contribute to CAF activation in high desmoplastic NSCLC.

Conclusions

Our findings demonstrate that functional heterogeneity of desmoplastic CAF is a determinant factor of NSCLC aggressiveness; thus, high desmoplastic CAFs represent a phenotypic subtype with a functional role for ST8SIA2 in promoting NSCLC invasion.

Acknowledgements

This work was supported by grants from the Canadian Institutes of Health Research (CIHR FDN148395 and MOP-115174), Canadian Cancer Society (#019293 and #020527), and the Ontario Ministry of Health and Long Term Care. Dr. Tsao is the M. Qasim Choksi chair in Lung Cancer Translational research. Dr. Cabanero was supported by the Terry Fox Foundation Training Program in Molecular Pathology of Cancer at CIHR (STP 53912). The data reported in this paper have been deposited into the Gene Expression Omnibus database; http://ncbi.nlm.nih.gov/geo/ (accession no. GSE116679).

Appendix A. Supplementary data

Supplementary data to this article can be found online at https://doi.org/10.1016/j.neo.2019.03.009.

References

[1] Navab R, Strumpf D, Bandarchi B, Zhu CQ, Pintilie M, Ramnarine VR, Ibrahimov E, Radulovich N, Leung L, and Barczyk M, et al (2011). Prognostic gene-expression signature of carcinoma-associated fibroblasts in non-small cell lung cancer. *Proc Natl Acad Sci U S A* **108**, 7160–7165.

[2] Navab R, Strumpf D, To C, Pasko E, Kim KS, Park CJ, Hai J, Liu J, Jonkman J, and Barczyk M, et al (2016). Integrin alpha11beta1 regulates cancer stromal stiffness and promotes tumorigenicity and metastasis in non-small cell lung cancer. *Oncogene.* **35**, 1899–1908

[3] Shekhar MP, Pauley R, and Heppner G (2003). Host microenvironment in breast cancer development: extracellular matrix-stromal cell contribution to

Figure 5. HD^{EX}-CAFs overexpressing *ST8SIA2* enhanced A549 NSCLC tumor cell invasion. (A) Western blot analysis for ST8SIA2. Western blot analysis of ST8SIA2 in three HD^{EX}-CAFs and three LD^{EX}-CAFs was studied for ST8SIA2 protein expression. β-Actin used for normalization. (B) The intensity of ST8SIA2 protein expression in HD^{EX}-CAFs and LD^{EX}-CAFs was normalized to its corresponding β-actin, and the ratio was plotted. (C) Using lentiviral strategy, ST8SIA2 shRNAs was infected in HD^{EX}-CAFs, and the level of *ST8SIA2* gene expression was measured by absolute qPCR. The values were normalized using the housekeeping gene *RPS13*. (D) Heterospheroids of ST8SIA2 shRNA-transfected HD^{EX}-CAFs + $A549^{dsred}$ or HD^{EX}-CAFs mock-transfected + $A549^{dsred}$ were embedded in collagen type I matrix, and the tumor cell invasion area was visualized after 2 days. A549 tumor cell invading area was analyzed by Image J. Full-length *ST8SIA2* cDNA was infected in HD^{EX}-CAFs (E) or in LD^{EX}-CAFs (G), and the level of *ST8SIA2* gene expression was measured. Heterospheroids of HD^{EX}-CAFs overexpressing ST8SIA2 + $A549^{dsred}$ (F) or LD^{EX}-CAFs overexpressing ST8SIA2 + $A549^{dsred}$ (H) were embedded in collagen type I matrix, and the tumor cell invasion area was analyzed. HD^{EX}-CAFs GFP-transfected + $A549^{dsred}$ or LD^{EX}-CAFs GFP-transfected + $A549^{dsred}$ were used as control. Statistical analysis for each data is provided in Supplementary data (Supplementary Table S17-19).

neoplastic phenotype of epithelial cells in the breast. *Breast Cancer Res* **5**, 130–135.
[4] Gonda TA, Varro A, Wang TC, and Tycko B (2010). Molecular biology of cancer-associated fibroblasts: can these cells be targeted in anti-cancer therapy? *Semin Cell Dev Biol* **21**, 2–10.
[5] Togo S, Polanska UM, Horimoto Y, and Orimo A (2013). Carcinoma-associated fibroblasts are a promising therapeutic target. *Cancers (Basel)* **5**, 149–169.
[6] Gascard P and Tlsty TD (2016). Carcinoma-associated fibroblasts: orchestrating the composition of malignancy. *Genes Dev* **30**, 1002–1019.
[7] Erez N, Truitt M, Olson P, Arron ST, and Hanahan D (2010). Cancer-associated fibroblasts are activated in incipient neoplasia to orchestrate tumor-promoting inflammation in an NF-kappaB–dependent manner. *Cancer Cell* **17**, 135–147.
[8] Servais C and Erez N (2013). From sentinel cells to inflammatory culprits: cancer-associated fibroblasts in tumour-related inflammation. *J Pathol* **229**, 198–207.
[9] Berdiel-Acer M, Sanz-Pamplona R, Calon A, Cuadras D, Berenguer A, Sanjuan X, Paules MJ, Salazar R, Moreno V, and Batlle E, et al (2014). Differences between CAFs and their paired NCF from adjacent colonic mucosa reveal functional heterogeneity of CAFs, providing prognostic information. *Mol Oncol* **8**, 1290–1305.
[10] Bhowmick NA, Neilson EG, and Moses HL (2004). Stromal fibroblasts in cancer initiation and progression. *Nature* **432**, 332–337.
[11] Costea DE, Hills A, Osman AH, Thurlow J, Kalna G, Huang X, Pena Murillo C, Parajuli H, Suliman S, and Kulasekara KK, et al (2013). Identification of two distinct carcinoma-associated fibroblast subtypes with differential tumor-promoting abilities in oral squamous cell carcinoma. *Cancer Res* **73**, 3888–3901.
[12] Ohlund D, Handly-Santana A, Biffi G, Elyada E, Almeida AS, Ponz-Sarvise M, Corbo V, Oni TE, Hearn SA, and Lee EJ, et al (2017). Distinct populations of inflammatory fibroblasts and myofibroblasts in pancreatic cancer. *J Exp Med* **214**, 579–596.
[13] Sugimoto H, Mundel TM, Kieran MW, and Kalluri R (2006). Identification of fibroblast heterogeneity in the tumor microenvironment. *Cancer Biol Ther* **5**, 1640–1646.
[14] Paulsson J and Micke P (2014). Prognostic relevance of cancer-associated fibroblasts in human cancer. *Semin Cancer Biol* **25**, 61–68.
[15] Amakye D, Jagani Z, and Dorsch M (2013). Unraveling the therapeutic potential of the Hedgehog pathway in cancer. *Nat Med* **19**, 1410–1422.
[16] Ozdemir BC, Pentcheva-Hoang T, Carstens JL, Zheng X, Wu CC, Simpson TR, Laklai H, Sugimoto H, Kahlert C, and Novitskiy SV, et al (2014). Depletion of carcinoma-associated fibroblasts and fibrosis induces immunosuppression and accelerates pancreas cancer with reduced survival. *Cancer Cell* **25**, 719–734.
[17] Rhim AD, Oberstein PE, Thomas DH, Mirek ET, Palermo CF, Sastra SA, Dekleva EN, Saunders T, Becerra CP, and Tattersall IW, et al (2014). Stromal elements act to restrain, rather than support, pancreatic ductal adenocarcinoma. *Cancer Cell* **25**, 735–747.
[18] Der SD, Sykes J, Pintilie M, Zhu CQ, Strumpf D, Liu N, Jurisica I, Shepherd FA, and Tsao MS (2014). Validation of a histology-independent prognostic gene signature for early-stage, non–small-cell lung cancer including stage IA patients. *J Thorac Oncol* **9**, 59–64.
[19] Gullberg D, Tingstrom A, Thuresson AC, Olsson L, Terracio L, Borg TK, and Rubin K (1990). Beta 1 integrin-mediated collagen gel contraction is stimulated by PDGF. *Exp Cell Res* **186**, 264–272.
[20] Osterholm C, Lu N, Liden A, Karlsen TV, Gullberg D, Reed RK, and Kusche-Gullberg M (2012). Fibroblast EXT1-levels influence tumor cell proliferation and migration in composite spheroids. *PLoS One* **7**e41334.
[21] Zhu CQ, Popova SN, Brown ER, Barsyte-Lovejoy D, Navab R, Shih W, Li M, Lu M, Jurisica I, and Penn LZ, et al (2007). Integrin alpha 11 regulates IGF2 expression in fibroblasts to enhance tumorigenicity of human non-small-cell lung cancer cells. *Proc Natl Acad Sci U S A* **104**, 11754–11759.
[22] Du P, Kibbe WA, and Lin SM (2008). lumi: a pipeline for processing Illumina microarray. *Bioinformatics* **24**, 1547–1548.
[23] Egeblad M, Nakasone ES, and Werb Z (2010). Tumors as organs: complex tissues that interface with the entire organism. *Dev Cell* **18**, 884–901.
[24] Levental KR, Yu H, Kass L, Lakins JN, Egeblad M, Erler JT, Fong SF, Csiszar K, Giaccia A, and Weninger W, et al (2009). Matrix crosslinking forces tumor progression by enhancing integrin signaling. *Cell* **139**, 891–906.
[25] Kim EJ, Sahai V, Abel EV, Griffith KA, Greenson JK, Takebe N, Khan GN, Blau JL, Craig R, and Balis UG, et al (2014). Pilot clinical trial of hedgehog pathway inhibitor GDC-0449 (vismodegib) in combination with gemcitabine in patients with metastatic pancreatic adenocarcinoma. *Clin Cancer Res* **20**, 5937–5945.
[26] Takahashi Y, Ishii G, Taira T, Fujii S, Yanagi S, Hishida T, Yoshida J, Nishimura M, Nomori H, and Nagai K, et al (2011). Fibrous stroma is associated with poorer prognosis in lung squamous cell carcinoma patients. *J Thorac Oncol* **6**, 1460–1467.
[27] Minami Y, Matsuno Y, Iijima T, Morishita Y, Onizuka M, Sakakibara Y, and Noguchi M (2005). Prognostication of small-sized primary pulmonary adenocarcinomas by histopathological and karyometric analysis. *Lung Cancer* **48**, 339–348.
[28] Herrera M, Islam AB, Herrera A, Martin P, Garcia V, Silva J, Garcia JM, Salas C, Casal I, and de Herreros AG, et al (2013). Functional heterogeneity of cancer-associated fibroblasts from human colon tumors shows specific prognostic gene expression signature. *Clin Cancer Res* **19**, 5914–5926.
[29] Su S, Chen J, Yao H, Liu J, Yu S, Lao L, Wang M, Luo M, Xing Y, and Chen F, et al (2018). CD10(+)GPR77(+) cancer-associated fibroblasts promote cancer formation and chemoresistance by sustaining cancer stemness. *Cell* **172**, 841–856 e816.
[30] Mesker WE, Junggeburt JM, Szuhai K, de Heer P, Morreau H, Tanke HJ, and Tollenaar RA (2007). The carcinoma-stromal ratio of colon carcinoma is an independent factor for survival compared to lymph node status and tumor stage. *Cell Oncol* **29**, 387–398.
[31] de Kruijf EM, van Nes JG, van de Velde CJ, Putter H, Smit VT, Liefers GJ, Kuppen PJ, Tollenaar RA, and Mesker WE (2011). Tumor-stroma ratio in the primary tumor is a prognostic factor in early breast cancer patients, especially in triple-negative carcinoma patients. *Breast Cancer Res Treat* **125**, 687–696.
[32] Harris AK, Stopak D, and Wild P (1981). Fibroblast traction as a mechanism for collagen morphogenesis. *Nature* **290**, 249–251.
[33] Sawhney RK and Howard J (2002). Slow local movements of collagen fibers by fibroblasts drive the rapid global self-organization of collagen gels. *J Cell Biol* **157**, 1083–1091.
[34] Rudnick JA, Arendt LM, Klebba I, Hinds JW, Iyer V, Gupta PB, Naber SP, and Kuperwasser C (2011). Functional heterogeneity of breast fibroblasts is defined by a prostaglandin secretory phenotype that promotes expansion of cancer-stem like cells. *PLoS One* **6**e24605.
[35] Cirri P and Chiarugi P (2012). Cancer-associated-fibroblasts and tumour cells: a diabolic liaison driving cancer progression. *Cancer Metastasis Rev* **31**, 195–208.
[36] Orimo A, Gupta PB, Sgroi DC, Arenzana-Seisdedos F, Delaunay T, Naeem R, Carey VJ, Richardson AL, and Weinberg RA (2005). Stromal fibroblasts present in invasive human breast carcinomas promote tumor growth and angiogenesis through elevated SDF-1/CXCL12 secretion. *Cell* **121**, 335–348.
[37] Kalluri R and Zeisberg M (2006). Fibroblasts in cancer. *Nat Rev Cancer* **6**, 392–401.
[38] Tlsty TD and Coussens LM (2006). Tumor stroma and regulation of cancer development. *Annu Rev Pathol* **1**, 119–150.
[39] Schreiber SC, Giehl K, Kastilan C, Hasel C, Muhlenhoff M, Adler G, Wedlich D, and Menke A (2008). Polysialylated NCAM represses E-cadherin–mediated cell-cell adhesion in pancreatic tumor cells. *Gastroenterology* **134**, 1555–1566.
[40] Ulm C, Saffarzadeh M, Mahavadi P, Muller S, Prem G, Saboor F, Simon P, Middendorff R, Geyer H, and Henneke I, et al (2013). Soluble polysialylated NCAM: a novel player of the innate immune system in the lung. *Cell Mol Life Sci* **70**, 3695–3708.
[41] Zhao Y, Li Y, Ma H, Dong W, Zhou H, Song X, Zhang J, and Jia L (2014). Modification of sialylation mediates the invasive properties and chemosensitivity of human hepatocellular carcinoma. *Mol Cell Proteomics* **13**, 520–536.
[42] Gong L, Zhou X, Yang J, Jiang Y, and Yang H (2017). Effects of the regulation of polysialyltransferase ST8SiaII on the invasiveness and metastasis of small cell lung cancer cells. *Oncol Rep* **37**, 131–138.
[43] Cazet AS, Hui MN, Elsworth BL, Wu SZ, Roden D, Chan CL, Skhinas JN, Collot R, Yang J, and Harvey K, et al (2018). Targeting stromal remodeling and cancer stem cell plasticity overcomes chemoresistance in triple negative breast cancer. *Nat Commun* **9**, 2897.